Available online at www.sciencedirect.com

SCIENCE DIRECT®

Solid State Ionics 176 (2005) 1–8

SOLID STATE IONICS

www.elsevier.com/locate/ssi

A photolithographic process for investigation of electrode reaction sites in solid oxide fuel cells

Erik Koep[a], Charles Compson[a], Meilin Liu[a,*], Zhiping Zhou[b]

[a]School of Materials Science and Engineering, Georgia Institute of Technology, Atlanta, GA 30332-0245 United States
[b]Microelectronics Research Center, Georgia Institute of Technology, Atlanta, GA 30332 United States

Received 29 April 2004; received in revised form 9 July 2004; accepted 21 July 2004

Abstract

Electrode kinetics greatly influence the overall performance of solid oxide fuel cells (SOFCs), especially at low temperatures. Yet little is known about the nature of SOFC electrode reactions. In this study, patterned electrodes of well-defined geometry were successfully deposited on YSZ ($Y_{0.08}Zr_{0.92}O_{2-\delta}$) electrolyte substrates through microfabrication techniques. Patterned LSM ($La_{0.8}Sr_{0.2}MnO_3$) microelectrodes were capped with a TiO_2 insulating layer in order to block the transport of ionic and electronic species across the surface thereby allowing separation of different reaction sites. The study confirms the feasibility of selectively blocking certain reaction sites in order to investigate complex electrochemical reaction mechanisms.

Keywords: Photolithographic process; Electrode reaction sites; Solid oxide fuel cells

1. Introduction

The recent entry of microelectrodes into solid-state ionics has allowed unique electrochemical characterization methods [1–10]. However, microelectrode manipulation and the resulting insight are not without problems [11,12]. While some valuable electrochemical insights have been gained, difficulties in fabrication and characterization have limited their use in solid-state electrochemistry. Microelectrodes provide a new method for understanding electrode kinetics, particularly oxygen reduction, though a practical and comprehensive process has proved elusive.

Reduction of oxygen involves a number of elemental steps such as adsorption of oxygen molecules, dissociation of molecules to atoms, ionization of oxygen molecules and combination of oxygen ions with oxygen vacancies. For an electrode made from a pure electronic conductor, such as platinum, the electrode reactions can occur only at or near the three-phase boundary (TPB), the region where gas phase meets electronic and ionic conducting phases at the electrode–electrolyte interface. In noble metal electrodes, all three necessary species—oxygen vacancies, electrons, and oxygen species in molecular, atomic, or ionic form (such as superoxide, peroxide, and oxide ions)—are available theoretically only at the TPB. In actuality, however, not only the transport of electrons along the surface of the electrolyte but also the motion of oxygen species (molecular, atomic, or ionic) along the surface of the metallic electrode may serve to slightly expand the TPB line to a reaction zone. Fig. 1(a–c) demonstrates schematically the competing reaction paths available for noble metal electrodes. In path (a), oxygen molecules directly adsorb at the one-dimensional TPB line and subsequently reduced to oxide ions and combine with oxygen vacancies. For path (b), oxygen may adsorb and be partially reduced on the electrode surface. The adsorbed species may then diffuse across the surface of the electrode to the TPB where it can be incorporated into the oxygen sublattice of the electrolyte. For path (c), oxygen may adsorb on the electrolyte surface and be subsequently reduced by electrons coming from the

* Corresponding author. Tel.: +1-404-894-6114; fax: +1-404-894-9140.
E-mail address: meilin.liu@mse.gatech.edu (M. Liu).

0167-2738/$ - see front matter © 2004 Elsevier B.V. All rights reserved.
doi:10.1016/j.ssi.2004.07.012

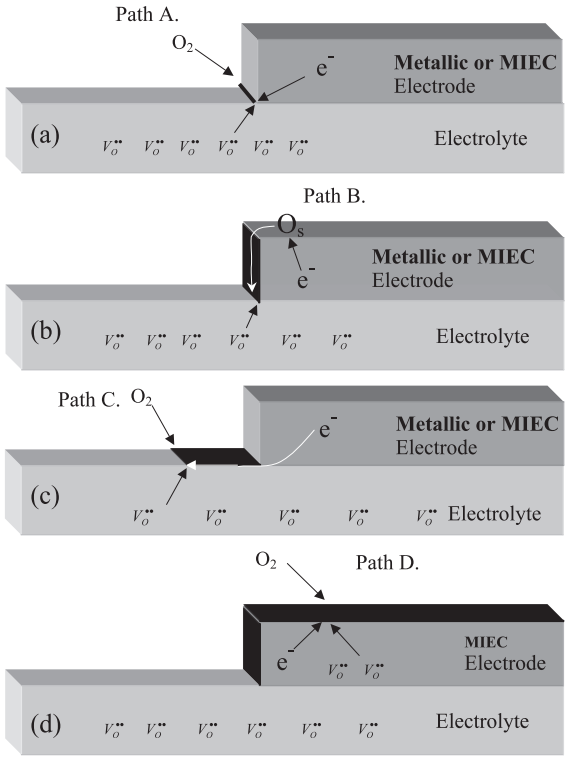

Fig. 1. Schematic of possible reaction pathways for electrodes in a solid-state electrochemical cell: (a) one-dimensional TPB along which oxygen, electrons, and oxygen vacancies may react directly, (b) electrode surface near TPB, where oxygen is adsorbed/partially reduced and subsequently diffuses along the electrode surface to the TPB in order to be incorporated into the oxygen sublattice, (c) oxygen may adsorb on the electrolyte surface and be subsequently reduced by electrons tunneling from the TPB along the surface of the electrolyte. Alternatively, the oxygen species adsorbed on electrolyte surface may transport to the TPB where they are reduced and combined with oxygen vacancies in the electrolyte; (d) oxygen species, electrons and oxygen vacancies react directly on an MIEC electrode surface far from the TPB.

TPB along the surface of the electrolyte. Alternatively, the oxygen species adsorbed on electrolyte surface may transport to the TPB where they are reduced and combined with oxygen vacancies in the electrolyte.

The use of a mixed ionic–electronic conductor (MIEC) as electrode is intended to dramatically expand the reach of the reaction zone across a larger, three-dimensional surface [13–18]. Due to the simultaneous transport of both ionic and electronic defects in MIECs, oxygen vacancies are able to migrate extended distances through the MIEC electrode. As a result, the effective reaction sites could be far beyond the three-phase boundary. In addition to reaction paths available to pure electronic conductors, as shown in Fig. 1(a–c), the simultaneous transport of both ionic and electronic defects through the MIEC allows a competing reaction path through the bulk of the MIEC electrode as schematically illustrated in Fig. 1(d). In this case, oxygen species may acquire both electrons and oxygen vacancies from the MIEC electrode at the same time, thereby allowing, in principle, oxygen reduction to occur anywhere on the entire MIEC electrode surface.

To date, however, the reaction rates on an MIEC electrode cannot be definitively attributed to either the three-phase boundary or reactions on the surface of the mixed conducting electrode [19]. The objective of this study was to develop a process capable of isolating particular active sites for reactions on an MIEC electrode, such as lanthanum strontium manganate ($La_{0.8}Sr_{0.2}MnO_3$) used in solid oxide fuel cells (SOFCs). Standard photolithographic techniques were used to pattern LSM electrodes with consistent surface area and triple phase boundary lengths [20]. An additional layer of TiO_2 was then deposited on top of the LSM electrodes to prevent ionic migration across the electrode roof. In this manner, micropatterned electrodes were used to explore the actual electrode reaction zone.

Recently, other experimental processes have been proposed that allow patterning of ceramic films down to submicron feature sizes on smooth surfaces [21,22]. While the method presented here does not currently boast similar feature sizes, it allows processing on rough surfaces, making it particularly applicable to SOFC systems in which the electrolyte surfaces are appreciably rougher than silicon-based substrates.

2. Experimental

Yttria-stabilized zirconia (YSZ) pellets prepared by tape casting were used as the substrates for patterned electrode and reference electrode deposition. YSZ powder from Daiichi, with a mean particle size of 0.26 μm, was suspended in a solvent-based slurry using Menhaden Fish Oil (dispersant), polyvinyl butyral (binder), poly-ethylene glycol (type I plasticizer) and butyl benzyl phthalate (type II plasticizer). The slurry was prepared in a two-stage milling process with at least 24 h between stages using 7-mm YSZ charge. Prior to casting, the slurry was de-aired by placing the jar in a vacuum chamber for about 5 min at −10″ Hg.

A stationary blade six-foot tabletop caster from Richard E. Mistler was used to cast the slurry at a blade height of about 150 μm. The tabletop caster was equipped with a DC motor, variable speed control, heated 5-ft casting bed, 1-ft^2 granite casting block, and counter directional mass-controlled airflow. The cast tape was then cut into 1.7-cm discs and laminated into stacks of three using a uniaxial press. Pellets were then sintered at 1400 °C for 5 h. The fired pellets experienced about 22% total shrinkage during firing as determined by dilatometry were about 400 μm thick according to SEM, and 95% of theoretical density as measured by the Archimedes method.

Electrodes were patterned onto the electrolyte surface utilizing standard photolithographic Lift-Off processing. Patterns for the desired electrodes were produced using AutoCAD software and transferred to chrome masks on glass plates. Identical electrodes were produced with electrode line widths of 50 μm within a surface area of 36

mm^2 for a total three-phase boundary (TPB) length of 2.05 m/cm^2.

Photolithography incorporated Microchem's 1805 photoresist into a process in which a CEE model 100 spinner was used to spin a consistent and uniform layer of photoresist onto the substrate. The 1805 resist was spun at 4000 rpm and softbaked on a hotplate at 120 °C for 3 min. Once the photoresist layer achieved sufficient uniformity and structure, the coated electrolytes were exposed under a Karl Suss MJB-3 Mask Aligner. Configuration of the exposure wavelength was selected to correspond to the optimal exposure range of the chosen photoresist. In this case, the recommended dosage of 150 mJ/cm^2 was sufficient for optimal processing.

Photoresist was developed through the use of Microchem's MF-319 Developer yielding good resolution of negative photoresist patterns. Dense LSM electrodes were developed through the use of a CVC Products RF Sputterer. A 3-in. diameter LSM target from Angstrom Sciences was purchased from Angstrom Sciences for deposition of the oxide films. Deposition rates showed very good consistency at 2.1 Å/s and SEM analysis of oxides revealed fully dense electrodes. Profilometer measurements confirmed a standard deviation in deposition depth of less than 9%. Fabrication of the titanium layer was accomplished through the use of a CVC Products Electron Beam Evaporator. The E-Beam Evaporator demonstrated good control of deposition thickness in addition to completely directional deposition, yielding a TiO_2 film thickness of 150 nm. Following deposition, the Lift-off method was completed by removing the PMGI and photoresist together with Microchem's Photoresist Remover in conjunction with ultrasonic bath. In-situ annealing of the patterned electrodes yielded a dense insulating titanium dioxide layer atop the conductive LSM patterned electrode.

In order to ensure that the TiO_2 layer did not approach the edge of the LSM patterned electrode, the TPB, the lithography process was modified by the use of a supplemental polydimethylglutarimide (PMGI) platform. Microchem's LOR 10B PMGI resist created an undercut platform that facilitated removal of the photoresist layer and ensured reliable definition of the TPB. The LOR was uniformly applied using the same CEE Model 100 spinner at 1700 rpm prior to application of the photoresist. The LOR was then softbaked on a hotplate at 190 °C for 6 min in order to solidify the platform.

LSM electrode thickness was controlled via determination and control of deposition rates. Patterned electrodes were 0.26 μm in height and completely dense. Since LSM is a relatively poor ionic conductor, thin electrodes were used to maximize the possibility of bulk diffusion. MIEC electrode patterns consisted of 60 identical rectangular patterned electrode strips (50 μm wide, 0.26 μm thick, and 6 mm long), connected through a lithographically processed current collector (dimension of 50 μm wide, 0.26 μm thick, and 6 mm long), to improve the reproducibility and reliability of the fabrication processes and electrochemical measurements. The smallest feature size of these patterned electrodes has been successfully reduced to about 2 μm.

In order to block the active site on the top surface of the MIEC electrode, an inactive layer of titanium dioxide was deposited on the top of a standard LSM patterned electrode. Density and thickness of TiO_2 layers were controlled in a similar fashion.

The cells consisted of a patterned electrode, covering an area of 6×6 mm, a reference electrode adjacent to the patterned electrode, and a counter electrode on the other side of the YSZ electrolyte prepared by painting and firing platinum paste (Hereaus LP11-4493). In order to ensure proper measurement, the reference electrodes were lithographically patterned and deposited with a maximum separation distance of 20 μm from the working electrode. Since the tape cast electrolyte was in excess of 250 μm thick, coplanar reference electrodes are adequate for separation of two electrode–electrolyte interfaces.

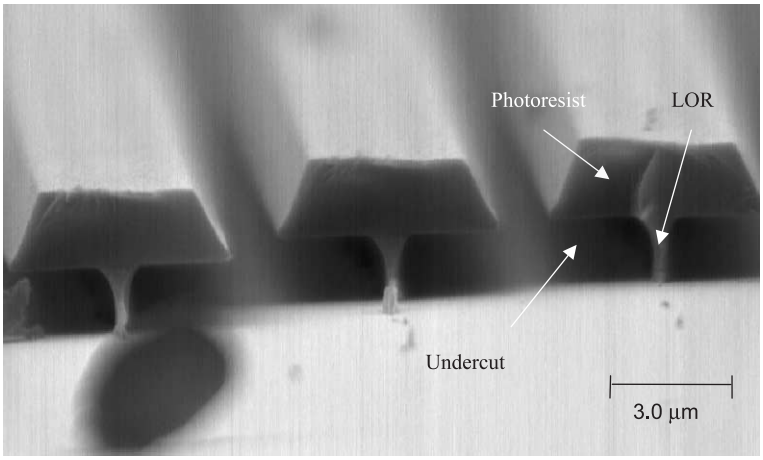

Fig. 2. A cross-sectional view (SEM micrograph) of a negative photoresist pattern showing the three-dimensional structure (Electrode strip width=1.5 μm, gap between two adjacent electrode strips=2.5 μm). Electrode material will be deposited in the gaps allowed between resist lines.

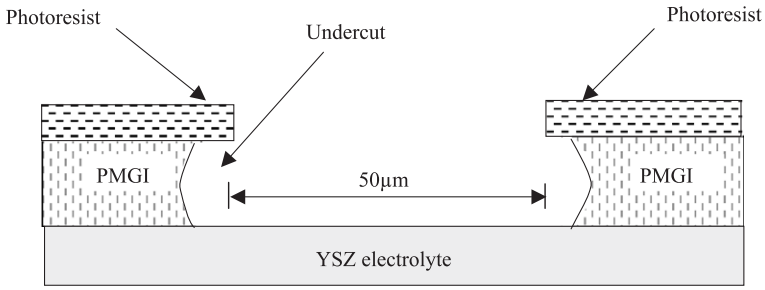

Fig. 3. A schematic cross-sectional view of a multi-layer negative photoresist pattern on an YSZ electrolyte. Please note the undercut separation from the edges of the pattern.

Cells were then placed in a tube furnace for impedance measurement at a constant temperature, ranging from 600 to 800 °C with 50 °C increments. A computer interface, controlling an EG&G 273A potentiostat and 5210 lock-in amplifier, collected impedance data over a range from 100 kHz to 0.01 Hz using both two- and three-electrode configurations.

3. Results and discussions

3.1. The desired negative resist pattern

Shown in Fig. 2 is a cross-sectional view (SEM micrograph) of an as-processed negative resist structure (dimension of 2.5 μm wide, 3 μm thick, and 6 mm long). It can be easily seen that the PMGI resist is undercut sufficiently back from the surface to avoid contact with the photoresist wall. This undercut allows good resolution of the TPB surface and provides the opportunity for multiple layer deposition.

Schematically shown in Fig. 3 is a cross-sectional schematic of the negative resist with a gap dimension of 50 μm wide and 3 μm thick for deposition of an MIEC electrode capped with an insulating layer but without blocking the TPBs. The large PMGI thickness, combined with a non-directional RF sputtering technique yielded MIEC electrodes slightly wider than the open region of the photoresist as determined by the mask. Since sputtering techniques deposit material from oblique angles, MIEC electrode dimensions are finalized slightly larger than mask dimensions. Consequently, subsequent deposition of an insulating layer from a directional source, in this case E-beam evaporation, yields a supplemental insulating film completely within the perimeter of the underlying electrode.

3.2. Deposition and photoresist removal

Schematically shown in Fig. 4 is a cross-sectional view of an MIEC (e.g., LSM) electrode capped with an insulating (e.g., TiO_2) layer after sequential depositions, produced by sputtering of the MIEC electrode (non-directional) followed by e-beam deposition of insulating layer (directional) using a negative resist (with dimension of 50 μm wide and 3 μm thick). Sputtering techniques are well known to cover edges and vertical walls during deposition. During sputtering, electrode material slowly builds up on the vertical walls of the photoresist layer, narrowing the gap for later deposition. This buildup serves to prevent the directional deposition layer from reaching the full outer limit of the pattern, even as defined by the mask.

Once deposition of desired materials has been completed, removal of the photoresist layers yields a patterned electrode of desired dimensions. The Lift-Off process ensures clean edges, necessary for quantifiable TPB length determination, along the entire length of the electrode. Schematically

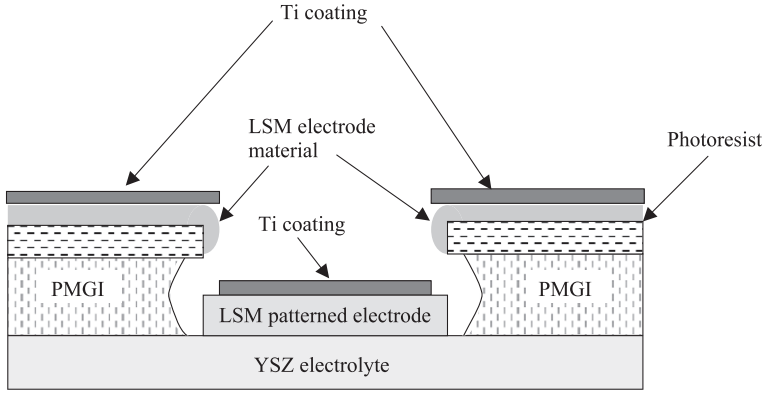

Fig. 4. A schematic cross-section of a cell with patterned electrodes before removal of photoresist. Notice that the LSM coating slightly covers the interior wall of the photoresist layer, creating a slightly smaller gap for the directional Ti layer.

shown in Fig. 5 is a cross-sectional view of the completed patterned electrode.

3.3. Selective blocking of reaction paths

Shown in Fig. 6 is a SEM micrograph of the same electrode construction as demonstrated in Fig. 5, viewed from above the surface. The edges of the TPB do not show any cracking or surface defects that would lead to increases in the actual TPB length. Furthermore, the edge of the titanium dioxide layer is smooth and uniformly recessed from the edge of the LSM electrode. Fig. 6 demonstrates good control, thereby selectively blocking only the active sites for oxygen reduction on the top surface of the electrode. This result is further confirmed via the EDXS dot-mapping shown in Fig. 7, indicating that the TiO_2 covers the entire surface of the LSM without crossing the TPB. Since the electrochemical activity of the TPB contributes to the overall performance, it is important to ensure that the TPBs are unimpeded by the TiO_2 layer. Precise electrode control was achieved through careful processing.

The most successful attempt so far to control bulk transport with blocking layers has been limited to circular disk electrodes. Brichzin et al. [9] demonstrated the effectiveness of an additional alumina layer serving to block ionic transport from the bulk into the electrolyte. In that case, the alumina layer was initially deposited directly onto the electrolyte. Subsequent deposition of the active electrode material yielded a three-dimensional structure with the blocking layer separating the electrode/electrolyte boundary.

Patterned arrays of microelectrodes developed via lift-off retain the electrochemical significance presented by Brichzin while simultaneously providing two distinct advantages. First, photolithography allows easy processing of a large matrix of interconnected patterned electrodes through the application of an overlaid current collector. Simultaneous lithography of the current collector also added a wire bond pad, thereby eliminating the need for an AFM tip for electrical contact. Contact areas for the electrodes were consistently reproducible in addition to being markedly easier to connect. Second, multiple electrodes now cover a significant area of the electrolyte, thereby averaging surface

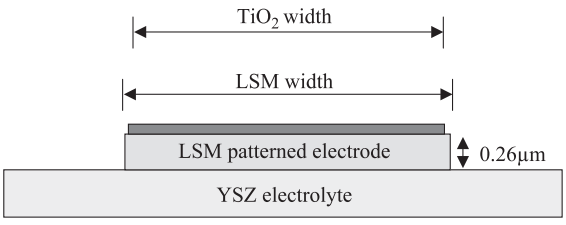

Fig. 5. A schematic cross-sectional view of patterned LSM capped with TiO_2 coating after removal of resist layers. The insulating coating effectively blocks ionic diffusion through the roof of the electrode. LSM width is slightly greater than 50 μm. TiO_2 width is slightly less than 50 μm.

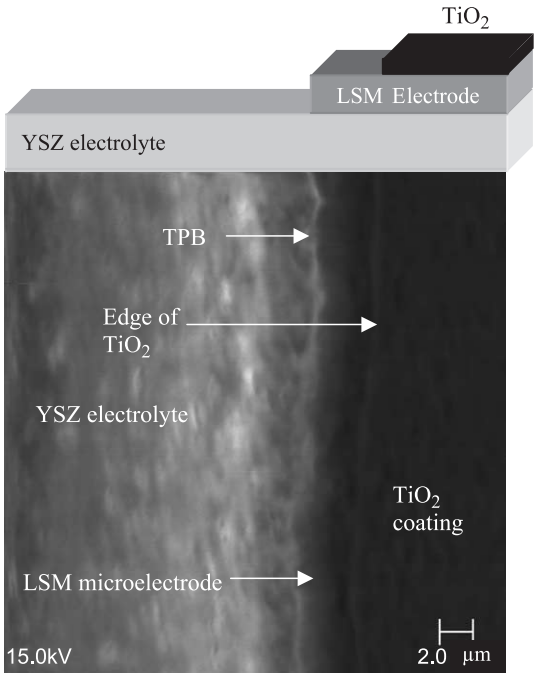

Fig. 6. Top-down SEM micrograph of Ti-coated LSM electrode. The TPB of LSM along YSZ can be clearly seen, as can the edge of the insulating layer.

anomalies. Patterned microelectrode arrays measure typical average properties, rather than atypical localized properties, thereby eliminating much of the additional complexity from site-specific microelectrodes. Since many studies seek a relationship between novel materials and overall electrochemical performance, this method may be more useful in some cases. Furthermore, larger amounts of reaction area lower total polarization resistance thus enhancing signal quality while using standard impedance analyzers [23,24].

By applying the insulating layer above the working electrode, as done here, transport across the MIEC top surface is effectively blocked, leaving only the TPB active for oxygen reduction. In this way, we are able to isolate the contribution from the TPB in relation to the bulk and surface effects. While it is unlikely that surface diffusion of adsorbed oxygen ions contributes significantly, by eliminating it from consideration, differentiation about the importance of the TPB can be achieved.

Furthermore, the method developed here may allow for determination of the location of the rate-limiting step. In addition to the ability to deposit blocking layers on the roof

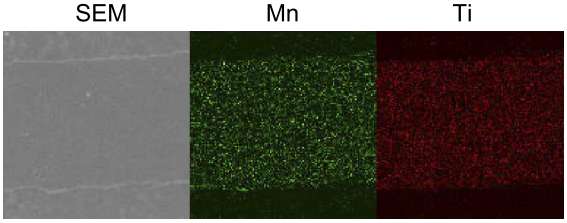

Fig. 7. EDXS dot mapping for TiO_2 capped LSM electrode. Electrode width and height are 50 and 0.26 μm, respectively.

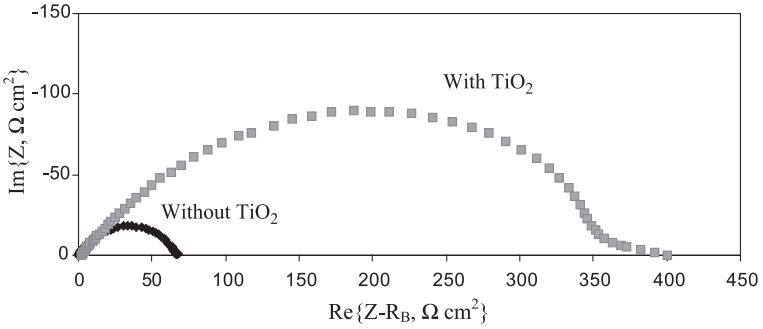

Fig. 8. Impedance spectra for uncapped and TiO_2 capped LSM electrode arrays measured at 750 °C.

of the electrode, the process can also be slightly altered to deposit blocking layers below the electrode. By simply switching the deposition order, an array of patterned electrodes similar to those presented by Brichzin can be produced without interrupting the TPB or surface diffusion. Since the current technique limits both bulk and surface diffusion, a reversal of deposition order would allow surface effects thereby yielding three experimental conditions for the three possible reaction paths.

Fleig [7], among others, has successfully modeled the equipotential lines of a dense MIEC electrode. These lines vary significantly in shape and breadth according to the location of the blocking layer. By comparing the electrochemical performance of patterned microelectrodes with blocking layers above and below the active electrode material, the relative importance of the electrode/atmosphere interface can be compared to that of the electrode/electrolyte interface.

3.4. Impedance spectroscopy of the patterned electrodes

Shown in Fig. 8 are some typical impedance spectra of the interfacial resistance between the electrolyte and the patterned LSM microelectrode with or without a TiO_2 layer. In this case, the impedance contribution from the electrolyte/counter electrode interface can be neglected since it accounts for less than 1% of the total interfacial resistance. The interfacial resistances were readily extracted through comparison of multiple configurations of two and three electrode measurements. Due to the use of a reference electrode, the cathode/electrolyte interfacial resistance can be taken from the intercepts of the impedance curve on the real axis. The impedance data clearly indicate that the impedance of the LSM electrode capped with a TiO_2 layer is much greater than that of the LSM electrode without a TiO_2 layer, implying that the simultaneous transport of electronic and ionic defects through the bulk phase of LSM makes an important contribution to oxygen reduction at the electrode. Both electrodes were patterned with the same thickness and TPB length, the only difference being the TiO_2 layer covering the electrode roof in selective cases. In both cases, the TPB region remained active and unimpeded. In the case of the TiO_2 capped electrode, surface adsorption on and bulk diffusion through the MIEC electrode were eliminated. Impedance results indicate a direct correlation between the interfacial polarization resistance and the contributions of different reaction path.

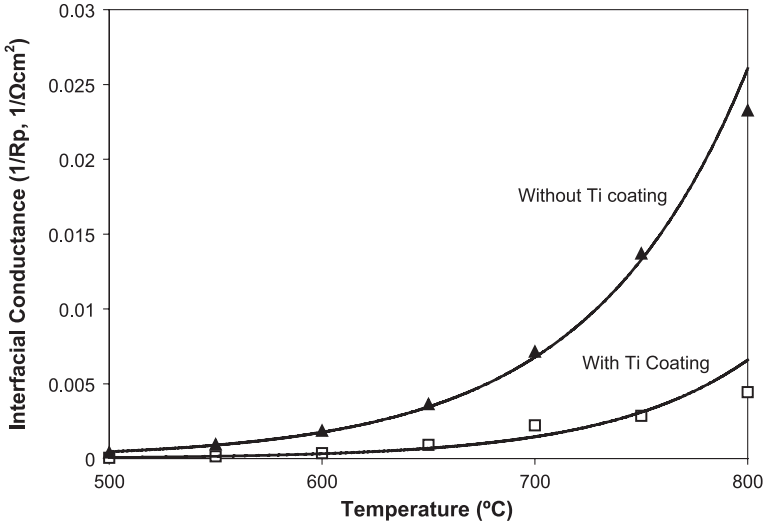

Fig. 9. Dependence of interfacial polarization resistance on temperature of two cells with LSM patterned electrodes (same TPB length and feature size) but with or without a TiO_2 coating.

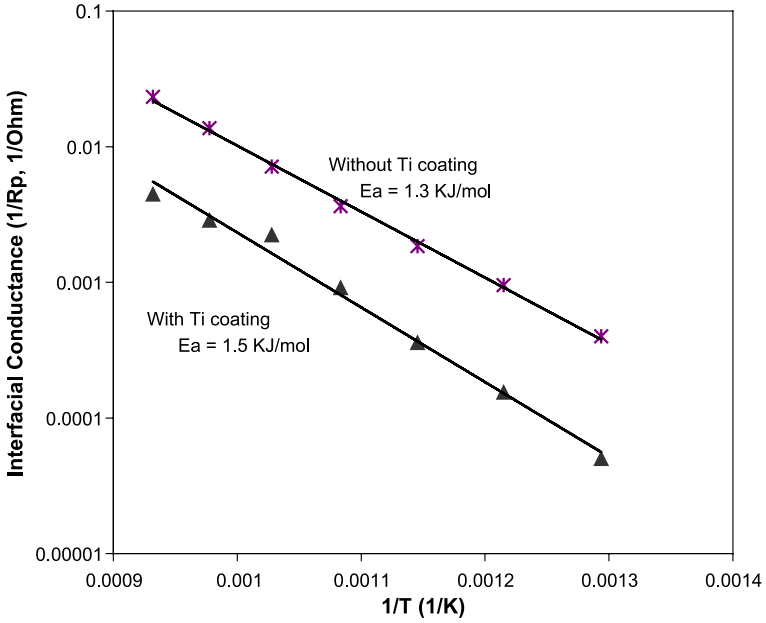

Fig. 10. Arrhenius plots for interfacial conductance of two LSM patterned electrodes (same TPB length and feature size) with or without a TiO_2 coating.

Shown in Fig. 9 is the dependence of the interfacial impedance on temperature at which the impedance spectra were acquired, indicating the increasing importance with temperature of ambipolar transport through the bulk phase of the MIEC. At low temperatures, the bulk path of the electrode does not contribute significantly even for very thin electrodes. However, the increased ambipolar transport through the bulk phase of the MIEC at high temperatures is reflected in the impedance data. Shown in Fig. 10 are the Arrhenius plots for the interfacial conductance (i.e., the reciprocal of the interfacial resistance). The calculated activation energies for the uncoated and TiO_2 coated LSM electrodes were 1.3 and 1.5 kJ/mol, respectively.

4. Conclusions

In this study, we have successfully developed a microfabrication process capable of producing well-defined three-dimensional geometries. SEM and EDXS micrographs confirm that a photolithographic process is indeed capable of producing patterned electrodes that satisfy the demands for accurate measurement. Furthermore, we have developed an improved procedure for selective determination of the relative importance of the MIEC surface in relation to the TPB. This cell provides a proof of concept towards the possibility of selecting particular components for study. By eliminating possible reaction paths, it may be possible to observe each individual path for reactions at an MIEC electrode, thereby completing a map of the reaction processes including relative contributions from each individual path.

The process presented here capitalizes on the many advantages of microelectrodes in solid-state ionics while simultaneously allowing for easier measurement and interpretation. Averaging over an array of microelectrodes yields performance results that depend on the comprehensive properties of the material rather than the specific characteristics of an individual microelectrode (strip or dot). For many studies, this would be a significant improvement as the information derived is more directly relevant to real systems. The process can be further expanded in order to determine the relative importance of the active sites for fuel cell reactions.

These initial findings were based solely on the use of dense LSM electrodes, but continued research is underway to expand the reach of this investigation to other mixed conducting electrodes, composites and three-dimensional structures. These further investigations should provide additional insight into active reaction sites, reaction mechanisms and better electrode architecture of mixed conducting electrodes. This process can be used to determine the active area for a variety of electrodes leading to direct improvements in electrode design.

Acknowledgements

This work was supported by DoE-NETL SECA Core Technology Program (Grant No. DE-FC26-02NT41572).

References

[1] H. Fukunaga, M. Ihara, K. Sakaki, K. Yamada, Solid State Ionics 86-88 (1996) 1179.
[2] T. Horita, K. Yamaji, N. Sakai, H. Yokokawa, T. Kato, J. Electrochem. Soc. 148 (2001) J25.

[3] T. Yammamura, H. Tagawa, T. Saito, J. Mizusaki, K. Kamitani, K. Hirano, S. Ehara, T. Takagi, Y. Hishinuma, H. Sasaki, T. Sogi, Y. Nakamura, K. Hashimoto, Solid State Ionics 70/71 (1994) 52.
[4] A. Mitterdorfer, L.J. Gauckler, Solid State Ionics, 117 Parts I and II (1999) 187 and 203.
[5] A. Bieberle, L.J. Gauckler, Solid State Ionics 135 (2000) 337.
[6] A. Bieberle, L.P. Meier, L.J. Gauckler, J. Electrochem. Soc. 148 (2001) A646.
[7] J. Fleig, Solid State Ionics 161 (3-4) (2003) 279.
[8] J. Fleig, J. Maier, Solid State Ionics 85 (1996) 9.
[9] V. Brichzin, J. Fleig, H.U. Habermeier, G. Cristiani, J. Maier, Solid State Ionics 152-153 (2002) 499.
[10] J. Fleig, J. Power Sources 105 (2002) 228.
[11] S. Rodewald, J. Fleig, J. Maier, J. Eur. Ceram. Soc. 19 (1999) 797.
[12] S.P. Jiang, J.G. Love, L. Apateanu, Solid State Ionics 160 (2003) 15.
[13] E. Maguire, B. Gharbage, F.M.B. Marques, J.A. Labrincha, Solid State Ionics 127 (2000) 329.
[14] T. Kawada, J. Suzuki, M. Sase, A. Kaimai, K. Yashiro, Y. Nigara, J. Mizusaki, K. Kawamura, H. Yugami, J. Electrochem. Soc. 149 (2002) E252.
[15] M. Mogensen, S. Skaarup, Solid State Ionics 86-88 (1996) 1151.
[16] Z.L. Wang, Z.C. Kang, Functional and Smart Materials, Plenum Press, New York, 1998.
[17] N.Q. Minh, T. Takahashi, Science and Technology of Ceramic Fuel Cells, Elsevier Science, Netherlands, 1995.
[18] E.P. Murray, T. Tsai, S. Barnett, Solid State Ionics 110 (1998) 235.
[19] M. Liu, J. Electrochem. Soc. 145 (1998) 142.
[20] M. Madou, Fundamentals of Microfabrication, CRC Press, Boca Raton, 1997.
[21] C.R. Martin, I.A. Aksay, J. Electroceramics 12 (2004) 53–68.
[22] M. Alexe, C. Harnagea, D. Hesse, J. Electroceramics 12 (2004) 69–88.
[23] M. Liu, J. Electrochem. Soc. 144 (1997) 1813.
[24] J. MacDonald, Impedance Spectroscopy, John Wiley and Sons, New York, 1987.